Chemistry & Biology *13*, 1307–1315, December 2006 DOI 10.1016/j.chembiol.2006.10.007

Structural and Antitumor Properties of the YSNSG Cyclopeptide Derived from Tumstatin

Jessica Thevenard,[1,4,7] Nicolas Floquet,[2,5,7,8] Laurent Ramont,[1,4] Elise Prost,[3,6] Jean-Marc Nuzillard,[3,6] Manuel Dauchez,[1,4] Hocine Yezid,[2,5] Alain J.P. Alix,[2,5] François-Xavier Maquart,[1,4] Jean-Claude Monboisse,[1,4] and Sylvie Brassart-Pasco[1,4,*]

[1] Laboratoire de Biochimie Médicale et Biologie Moléculaire
CNRS UMR 6198
IFR 53 Biomolécules
Université de Reims Champagne-Ardenne
51095 Reims
France

[2] Laboratoire de Spectroscopies et Structures BioMoléculaires
IFR 53 Biomolécules
Université de Reims Champagne-Ardenne
51687 Reims Cedex 2
France

[3] Isolement, Structure, Transformations et Synthèse de Substances Naturelles
CNRS FRE 2715
IFR 53 Biomolécules
Université de Reims Champagne-Ardenne
51096 Reims
France

Summary

We previously demonstrated that the NC1[α3(IV)185–191] CNYYSNS peptide inhibited in vivo tumor progression. The YSNS motif formed a β turn crucial for biological activity. The aim of the present study was to design a YSNSG cyclopeptide with a constrained β turn on the YSNS residues more stable than CNYYSNS. By nuclear magnetic resonance and molecular modeling, we demonstrated that the YSNSG cyclopeptide actually adopted the expected β-turn conformation. It promoted melanoma cell adhesion and prevented their adhesion to the native peptide. It inhibited in vitro cell proliferation and migration through Matrigel by downregulating proteolytic cascades. Moreover, intraperitoneal administration of the YSNSG cyclopeptide inhibited melanoma progression far more efficiently than the native peptide. The increased solubility and stability at low pH of the YSNSG cyclopeptide suggest this peptide as a potent antitumor therapeutic agent.

Introduction

Tumor invasion and metastasis require proteolytic degradation of extracellular matrix (ECM). This degradation involves various proteolytic cascades, such as matrix metalloproteinase (MMP) activation and the plasminogen activation system. MMPs belong to a zinc-dependent proteinase family with more than 25 members, secreted as inactive zymogens [1, 2]. Their activation, a major step in tumor invasion, results from an imbalance between levels of tissue inhibitors of metalloproteinases (TIMPs) and MMP activators, such as urokinase, plasmin, or membrane type MMPs (MT-MMPs). The latter constitutes an MMP subfamily containing an additional anchor domain which links the enzyme to the plasma membrane. MT-MMPs actively participate in the basement membrane degradation either directly or by activating latent pro-MMP-2 and pro-MMP-13 [3–5]. The plasminogen activation system, composed of two different plasminogen activators, urokinase-type plasminogen activator (uPA) and tissue-type plasminogen activator (t-PA), both controlled by plasminogen activator inhibitors (PAI-1 and PAI-2), is also actively involved in basement membrane degradation either by direct breakdown of ECM macromolecules or by activating pro-MMPs [6, 7].

Basement membranes are essentially composed of type IV collagen, laminins, entactin/nidogen, and heparan sulfate proteoglycans. Type IV collagen is organized as a network of heterotrimers composed of three α(IV) chains among six possible, α1(IV) to α6(IV), each encoded by a specific gene [8]. Each chain comprises a 7S domain at its N terminus, a large central triple-helical domain of about 1400 amino acids, and a C-terminal noncollagenous (NC1) domain of about 240 amino acids. It is now recognized that NC1 domains from type IV collagen, but also from other collagen types, display several biological activities, mainly regulating tumor invasion and angiogenesis in various cancer types [9]. NC1 α3(IV) chain, also called tumstatin, was first shown by Maeshima et al. to display antiangiogenic properties [10].

In previous studies, we demonstrated that the NC1[α3(IV)185–203] peptide exhibits both in vitro and in vivo antitumor properties [11, 12]. A shorter CNYYSNS peptide, corresponding to residues 185–191, shared the same antitumor properties. The peptide adopts a β-turn conformation crucial for its biological activity. The aim of the present study was to design a peptide that contains both the four residues forming the YSNS β turn and a glycine residue allowing cyclization to constrain the β-turn conformation, to increase peptide stability and therefore to increase its biological activity. By nuclear magnetic resonance (NMR) and molecular modeling, we demonstrated that the YSNSG cyclopeptide actually adopts the expected β-turn conformation and exhibits antitumor properties.

*Correspondence: sylvie.brassart-pasco@univ-reims.fr
[4] Lab address: http://helios.univ-reims.fr/Labos/LBMBM/
[5] Lab address: http://helios.univ-reims.fr/Labos/LSSB/
[6] Lab address: http://helios.univ-reims.fr/Labos/UPRESA6013/
[7] These authors contributed equally to this work.
[8] Present address: Institut de Chimie des Substances Naturelles, CNRS UPR 2301, 91198 Gif-sur-Yvette, France.

Results and Discussion

Structure of the YSNSG Linear Peptide

As a starting point of our study, a molecular dynamics simulation (MDS) was performed at 300K on the linear YSNSG peptide, either without or with an explicit representation of the solvent and starting from a fully extended conformation. The first MDS in implicit solvent lasted 50 ns. The main result obtained was the observation of stable β turns of type I (canonical or close) on YSNS and/or SNSG (50% of the conformations).

The second MDS in explicit solvent lasted 20 ns. As a final result, ten clusters (representative structures) were deduced from the trajectory (data not shown). Among these clusters, the presence of a YSNS β turn, an SNSG β turn, intermediate structures, and structures of extended or quasi-extended conformations could be noted. According to their φ/ψ, the YSNS and the SNSG β turns were found to be very close to two compatible type I β turns, in perfect agreement with standard prediction [13].

Structure of the YSNSG Cyclopeptide

First, an MDS of the YSNSG cyclopeptide was performed under the same conditions as the ones computed for the linear YSNSG peptide. The main result obtained was the observation, for the five residues, of dihedral angles characteristic of type I β turns (canonical or close) along all the 50 ns of the trajectory, indicating a stable conformation with a rather rigid backbone.

Second, the YSNSG cyclopeptide structure was analyzed by NMR. After assignment of all the proton signals on the TOCSY spectrum, some of the most interesting information came from the NOESY spectrum, which clearly indicated correlation between the backbone amide protons of sequential residues whereas no correlation was observed for nonsequential ones. A few other nuclear Overhauser effects (nOes) were also revealed by the spectra, in the NH-Hα region (data not shown).

A random conformational search of the peptide structure was performed under NMR distance constraints (see Experimental Procedures). Interestingly, the three independent runs converged to the same conformation of lowest energy, with an rmsd on all atoms less than 0.2 Å. This structure (Figure 1) shared a β turn on the YSNS residues, with a Cα(Y_1)-Cα(S_4) distance less than 7.0 Å. This structure in implicit solvent was stabilized both by an H bond between the amide proton of tyrosine Y_1 and the C=O of serine S_4, forming a γ turn on the S_4GY_1 residues, and by an H bond between the hydroxyl group of Y_1 and the side chain amide function of asparagine N_3.

This conformation was further used as a starting point for an unconstrained MDS that was performed under the same conditions as those computed for the linear YSNSG peptide (explicit water, 300K). As expected, the cyclopeptide was observed as highly constrained, as indicated by a rmsd value less than 0.5 Å on its backbone atoms throughout the trajectory (data not shown). The γ turn described above quickly disappeared (during the heating phase) to reach another stable conformation. Flexibility of the peptide was further reduced to the exploration of the different rotamers of the tyrosine (Figure 2A). The corresponding conformation was characterized by a YSNS β turn along the entire trajectory (Figure 2B). Plotting the φ and ψ angles of the peptides versus time also showed that the five residues were often located in the α-helical region of the Ramachandran map, making the YSNS tetrapeptide close to a type I β turn (Figure 2C). However, senso stricto, this turn did not belong to any of the canonical types of β turn with mean φ/ψ of (−90°; −66°) for both serine S_2 and asparagine N_3 residues.

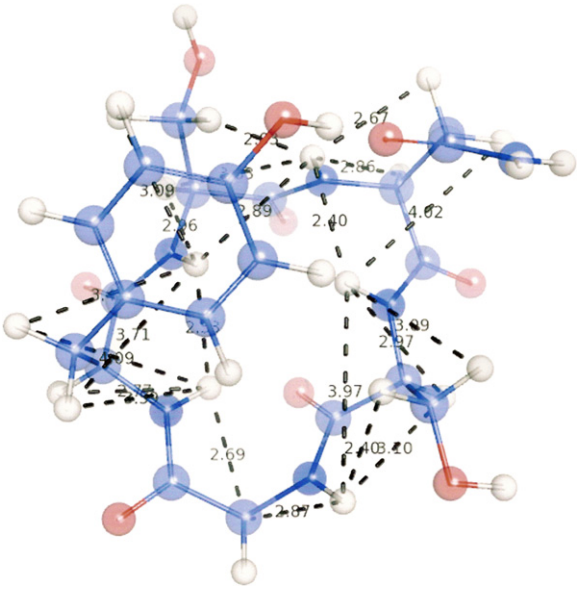

Figure 1. Minimal Energy Conformation of the YSNSG Cyclopeptide

This conformation shares the lowest potential energy and comes from the random conformational search of the YSNSG cyclopeptide in implicit solvent (using a distance-dependent dielectric constant). This structure is built in agreement with our NMR data (experimentally observed nOes that were included as constraints during the minimization process are reported as dashed lines).

This conformation was very close to a β turn spanning the YSNS sequence described for the linear YSNSG peptide with a mean rmsd of ~1.5 Å calculated on backbone atoms.

Comparison between Theoretical and Experimental Data of the YSNSG Cyclopeptide

To compare our theoretical and experimental results thoroughly, some proton-proton average distances extracted from the MDS were plotted (Figure 3). All the nOes observed experimentally, especially between the amide protons of sequential residues, corresponded to mean distances less than 4.0 Å; on the contrary, the amide protons of the backbone that did not correlate also corresponded to distances greater than 4.0 Å. Moreover, we observed that mean values of φ dihedral angles of the two serine residues were about −90°, in agreement with the NMR experiment (−120° ± 30°).

One particular aspect of the conformation of the peptide observed along the molecular dynamics trajectory is that all the NHs of its backbone were grouped on the same side, whereas all the carbonyl groups were grouped on the other side (Figure S1 in the Supplemental Data available with this article online). This specific

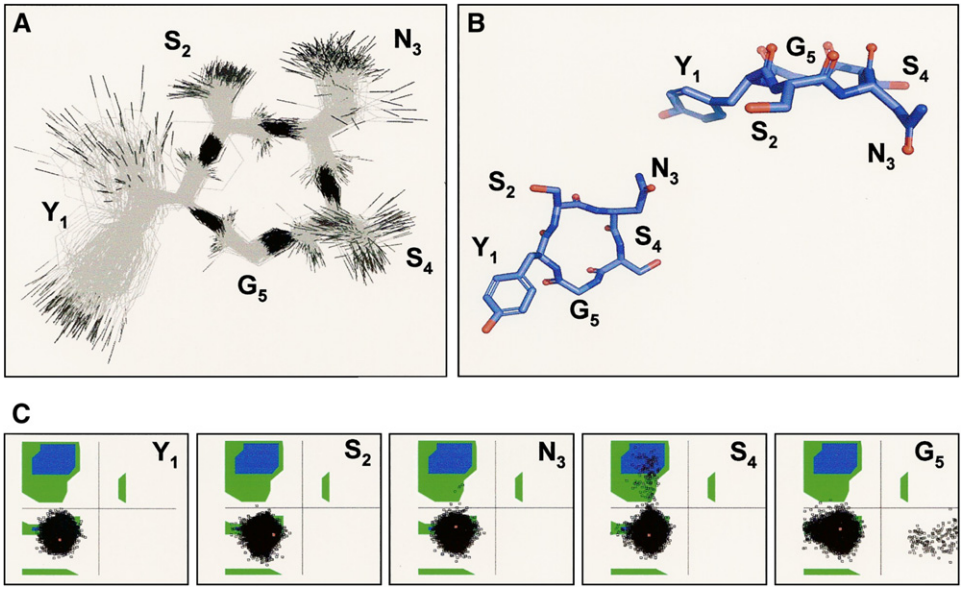

Figure 2. The Stable Structure of the YSNSG Cyclopeptide as Observed along the 20 ns Molecular Dynamics Trajectory

The simulation is performed in an explicit water box and shows a stable YSNS β turn.

(A) Flexibility of the peptide is reduced to the tyrosine side chain.

(B) The stable structure of the peptide, characterized by a YSNS β turn along the entire trajectory, presents the particularity to separate NH and C=O of its backbone on each of its sides, also preventing internal H bonds.

(C) Plotting the φ and ψ angles of the peptides shows that the five residues are often located in the α-helical region of the Ramachandran map, with mean φ/ψ of (−90°; −66°) for both serine S_2 and asparagine N_3 residues, making the YSNS tetrapeptide close to a type I β turn.

feature prevents the formation of backbone internal hydrogen bonds, in agreement with the NMR experimental data. The temperature coefficients of the amide protons of the peptide, which were recorded between 295K and 320K, failed to reveal any internal H bond, with values of −10.0, −4.6, −7.0, −4.6, and −6.1 ppb/K for Y_1, S_2, N_3, S_4, and G_5, respectively (usually values < −4.5 ppb/K correspond to the absence of an H bond) (Figure S1). Thus, the peptide appears to be highly polarized, as shown by the electrostatic potential of the cyclopeptide (isovalues of +7.5 and −7.5 kT/e in blue and red, respectively). The charge distribution was computed by using

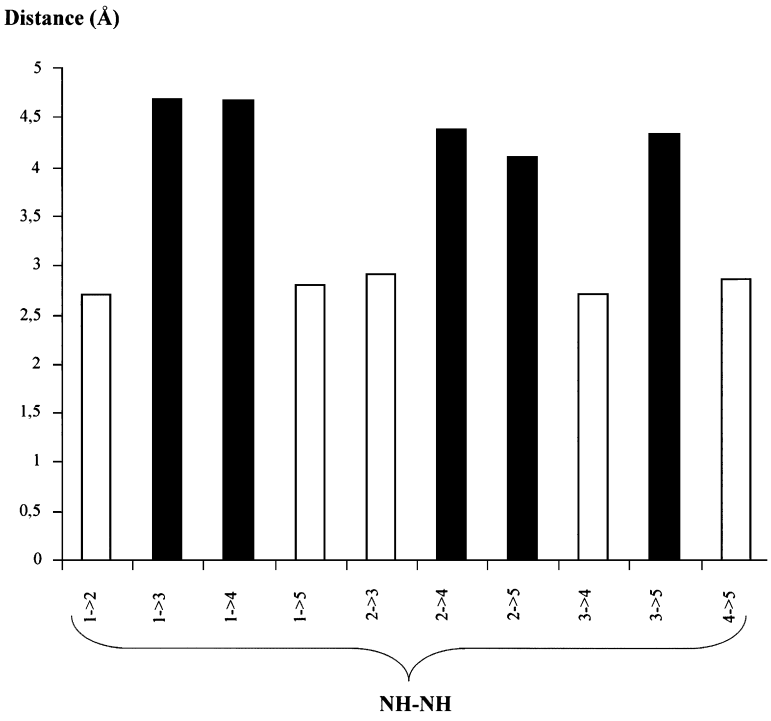

Figure 3. Comparison of Experimental and Theoretical Proton-Proton Distances of the YSNSG Cyclopeptide

The nOes experimentally obtained are reported in white and the theoretical in black. The mean proton-proton distances are extracted from trajectories of the molecular dynamic simulations performed on the YSNSG cyclopeptide.

the default parameters of the particle mesh Ewald method [14] as implemented in VMD [15]. Interestingly, the positive charges encompassed the side chains of the SNS residues that are known to be crucial for biological activity of the native peptide or its derivatives, a feature that may also be important for its binding to αVβ3 integrin [16].

Secondary Structure Characterization by Electronic Circular Dichroism Spectroscopy

The circular dichroism (CD) spectra of the YSNSG cyclopeptide recorded at pH 7 and at various temperatures did not clearly demonstrate the presence of an ordered conformation. The same results were observed without adding any buffer, also keeping a pH of 3; this showed a poor sensitivity of the peptide to temperature and pH, probably due to its highly constrained conformation (data not shown). The observed CD shape is therefore not characteristic of any of the classical β-turn conformations (type I, type II, or type VIII); this is probably due to the distorted φ/ψ of the peptide as compared to a type I β turn.

NMR and molecular modeling results showed that the YSNSG cyclopeptide actually adopted the expected β-turn conformation on the YSNS residues. This conformation did not depend on temperature and pH, suggesting a higher stability than that of the native peptide. It also showed the particularity that all its peptide bonds are in *trans* conformation without any internal H bond; indeed, all its amine and carboxyl backbone groups were grouped on opposite sides of the peptide. This distribution pattern of electrostatic potential is an important feature that should be taken into consideration for the binding of the cyclopeptide to αVβ3 integrin.

In the second part of the study, we compared YSNSG cyclopeptide biological activity to that of the native CNYYSNS peptide.

Effect of the YSNSG Cyclopeptide on UACC-903 Human Melanoma Cell Adhesion, Proliferation, and Migration

The native CNYYSNS peptide (NP7) and the YSNSG cyclopeptide (C5) promoted UACC-903 melanoma cell adhesion like the NC1[α3(IV)185–203] peptide (Figure 4A). Cell adhesion was inhibited by a preincubation of melanoma cells with an anti-αVβ3 integrin antibody, whereas an anti-β1 antibody had no effect (data not shown). This result confirms that, like NP7 [16], C5 interacts with αVβ3 integrin. Competition assays demonstrated that, like the NC1[α3(IV)185–203] peptide [16], NP7 and C5 also inhibited the adhesion of UACC-903 cells to NC1[α3(IV)185–203]-coated culture plates. The treatment of melanoma cells with the NC1[α3(IV)185–203] also prevented their adhesion to both NP7 and C5. This result suggests that C5 binds to αVβ3 integrin at the same site as the NP7 and NC1[α3(IV)185–203] peptides.

Tumor progression depends on cell proliferation and migration. The in vitro proliferation of UACC-903 human melanoma cells was significantly inhibited by the CNYYSNS peptide (−45%). The YSNSG cyclopeptide at 5, 10, and 20 μM also inhibited UACC-903 melanoma cell proliferation by 27%, 29%, and 40%, respectively (Figure 4B). The cyclopeptide was as efficient as the native peptide at the same concentration. The effect of the YSNSG cyclopeptide on UACC-903 cell migration through an in vitro-reconstituted basement membrane

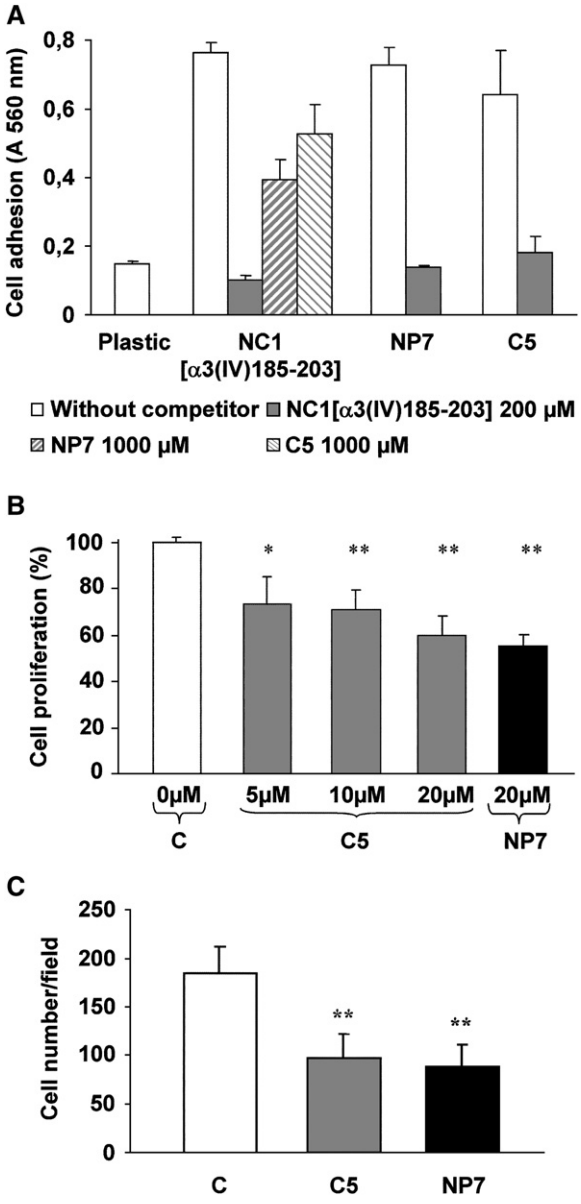

Figure 4. Effect of the YSNSG Cyclopeptide on UACC-903 Melanoma Cell Adhesion, Proliferation, and Migration

(A) UACC-903 melanoma cell adhesion is measured after nuclei staining with crystal violet. Cells are seeded onto plastic, native NC1[α3(IV)185–203] peptide-, native CNYYSNS peptide NP7-, or YSNSG cyclopeptide C5-coated plates with or without preincubation with competitors.

(B) UACC-903 cell proliferation is determined using WST-1 reagent. Cells are incubated in 24-well culture plates for 48 hr with either control medium (C), YSNSG cyclopeptide (C5), or CNYYSNS native peptide (NP7).

(C) UACC-903 cell invasion is assayed in modified Boyden chambers. After a 72 hr incubation period, migrated cells are stained with crystal violet and counted with an inverted microscope.

C, control; C5, YSNSG cyclopeptide (20 μM); NP7, CNYYSNS native peptide (20 μM).

*, significantly different from control at $p < 0.05$. **, significantly different from control at $p < 0.01$.

was analyzed using Matrigel-coated membranes and 10% fetal calf serum as a chemoattractant. Migration was assessed after 72 hr. The YSNSG cyclopeptide (20 μM) induced a 47% decrease of UACC-903 cell migration, similar to the CNYYSNS peptide at the same concentration (Figure 4C).

Effect of the YSNSG Cyclopeptide on Matrix Metalloproteinases and Their Inhibitors

The matrix metalloproteinase activation cascade is largely involved in ECM degradation.

No significant changes in MMP-2 and MMP-9 secretion were detected by gelatin zymography on cell media after incubation of the UACC-903 cells with either the YSNSG cyclopeptide or the native CNYYSNS peptide (data not shown).

Secretion of TIMPs into the conditioned culture medium was analyzed by reverse zymography. A dose-dependent increase in TIMP-2 secretion was observed in the cultures incubated with YSNSG cyclopeptide, as well as with CNYYSNS (Figure 5A). An ELISA measurement of TIMP-2 secretion also confirmed this result (data not shown). TIMP-1 and TIMP-3 secretion were not altered.

The YSNSG cyclopeptide strongly inhibited pro-MMP-14 expression, as demonstrated by western blot analysis (Figure 5B). Pro-MMP-14 activation was also completely abolished. The inhibitory effects of the cyclopeptide were of the same intensity as the native peptide. The treatment of UACC-903 cells with either the YSNSG cyclopeptide or the native CNYYSNS peptide also largely decreased the binding of pro-MMP-2 to tumor cell membrane and its activation (Figure 5C).

MMP-14 is able to degrade ECM (types I–III collagens, fibronectin, laminins, fibrin, gelatin, nidogen, and cartilage proteoglycan core proteins). It is inhibited by TIMP-2 [17]. In our model, TIMP-2 secretion was significantly increased by incubation with either the YSNSG cyclopeptide or the native CNYYSNS peptide. The expression and activation of MMP-14 were also strongly inhibited, leading to a large decrease in the activation of pro-MMP-2 associated with tumor cell membrane. This should explain, at least partially, the strong reduction in the invasive capacities of melanoma cells.

Effect of the YSNSG Cyclopeptide on the Plasminogen Activation System

Another proteolytic cascade involved in tumor invasion is the activation of plasminogen into plasmin by plasminogen activators u-PA and t-PA [6]. Secretion of u-PA and t-PA was analyzed by gelatin-plasminogen zymography (Figure 6A). Treatment of UACC-903 cells with the YSNSG cyclopeptide induced a dose-dependent decrease in both u-PA and t-PA secretion, up to −56% and −55%, respectively, more efficiently than the native CNYYSNS peptide (−40% and −48%, respectively). Secretion of PAI-1, the u-PA and t-PA inhibitor, was analyzed by western blot (Figure 6B). Treatment of UACC-903 cells with the YSNSG cyclopeptide (20 μM) induced a 4.0-fold increase in PAI-1 secretion versus a 3.4-fold increase with the native CNYYSNS peptide at the same concentration.

Collectively, the inhibition of MMP-2/MMP-14 and plasminogen activation may explain most of the decrease in ECM degradation and the inhibition of in vitro tumor cell migration.

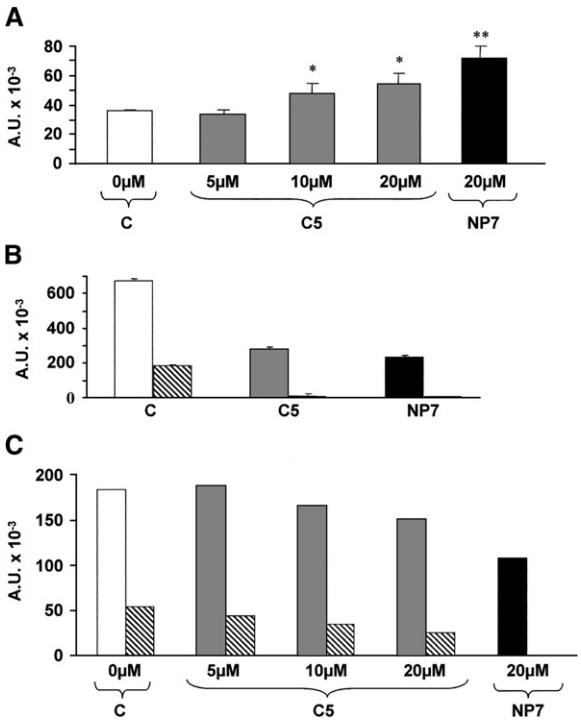

Figure 5. Effect of the YSNSG Cyclopeptide on the Pro-MMP-2 Activation Cascade

UACC-903 melanoma cells are incubated for 48 hr with control medium (C), YSNSG cyclopeptide (C5), or CNYYSNS native peptide (NP7).

(A) TIMP secretion is analyzed by reverse zymography on conditioned media.

(B) MMP-14 expression and activation in cell extracts are analyzed by western blot (pro-MMP-14, empty bars; MMP-14, hatched bars).

(C) Pro-MMP-2 activation in cell extracts is analyzed by gelatin zymography (pro-MMP-2, empty bars; MMP-2, hatched bars).

Quantifications are performed by densitometry using Bio-1D software (Vilber Lourmat, Marne-la-Vallée, France). Results are expressed as arbitrary units (A.U.).

*, significantly different from control at $p < 0.05$. **, significantly different from control at $p < 0.01$.

Inhibition of In Vivo Tumor Growth by the YSNSG Cyclopeptide

In previous studies [12], we demonstrated that the peritumor injection of the native CNYYSNS peptide inhibited tumor growth. In the current paper, we used other experimental conditions. Melanoma cells were subcutaneously injected into the left side of syngenic C57BL6 mice. Tumors appeared at day 6. Intraperitoneal injections of either native CNYYSNS peptide or YSNSG cyclopeptide were performed at day 6, 8, and 11 (10 mg/kg). Tumors were measured at day 14 (Figure 7). The YSNSG cyclopeptide inhibited tumor cells by 46% and the native CNYYSNS peptide by 27%, strongly suggesting that the cyclopeptide is more stable than the native peptide after systemic administration.

The design of cyclic RGD-containing peptides to antagonize αVβ3 integrin clearly demonstrated that cyclization confers to these peptides a large increase in

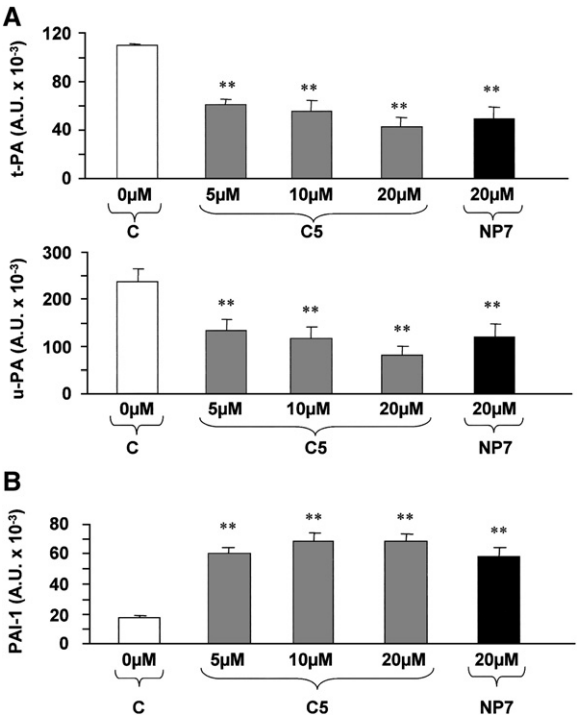

Figure 6. Inhibition of Plasminogen Activator Secretion by the YSNSG Cyclopeptide

UACC-903 melanoma cells are incubated for 48 hr with control medium (C), YSNSG cyclopeptide (C5), or CNYYSNS native peptide (NP7).

(A) u-PA and t-PA secretion into the conditioned media are analyzed by gelatin-plasminogen zymography.

(B) PAI-1 secretion into the conditioned media is analyzed by western blot.

Quantifications are performed by densitometry using Bio-1D software. Results are expressed as arbitrary units (A.U.).

**, significantly different from control at $p < 0.01$.

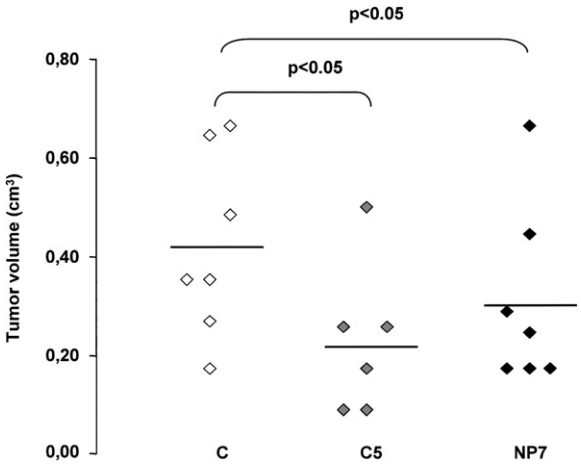

Figure 7. Inhibition of In Vivo Tumor Growth by the YSNSG Cyclopeptide

B16F1 cells are subcutaneously injected into syngenic C57BL6 mice (2.5×10^5 cells per mouse). Intraperitoneal administrations of either YSNSG cyclopeptide (C5) or CNYYSNS native peptide (NP7) (10 mg/kg) are performed at day 6, 8, and 11. Tumor volume is measured at day 14. Statistical significance is determined using the nonparametric *u*-test of Mann and Whitney.

their resistance to proteolytic degradation and an improved bioavailability as reported in the literature [18–20]. This is in agreement with our results suggesting a higher stability of the YSNSG cyclopeptide versus the native CNYYSNS peptide. Our experimental data also confirmed that the binding of tumstatin-derived peptides to αVβ3 integrin requires a β turn located on the YSNS residues. The tumstatin-derived peptides act as αVβ3 integrin antagonists.

The cyclic conformation of the YSNSG peptide and its stability at low pH should suggest this peptide as a potent antitumor therapeutic agent which might be administered per os or intraperitoneally.

Significance

Increasing interest is presently devoted to specific domains of extracellular matrix macromolecules which are able to regulate cell activities (matrikines). Type IV basement membrane collagen was recently demonstrated to be a source of various matrikines which may play an important role in limiting cancer progression. The C-terminal noncollagenous NC1 domains from type IV collagen inhibit tumor invasion and/or angiogenesis in various cancer types. We previously demonstrated that the CNYYSNS sequence from the NC1 domain of type IV collagen α3 chain inhibited tumor progression in an in vivo mouse melanoma model, through binding to αVβ3 integrin. The YSNS residues formed a β turn crucial for biological activity. The aim of the present study was to design a YSNSG cyclopeptide with a constrained β turn on the YSNS residues, more active and stable than native CNYYSNS. By nuclear magnetic resonance and molecular modeling, we demonstrated that the YSNSG cyclopeptide actually adopted the expected β-turn conformation and inhibited melanoma cell proliferation and invasive properties as well as the native CNYYSNS peptide. Moreover, intraperitoneal administration of the YSNSG cyclopeptide after tumor development inhibited melanoma progression far more efficiently than the native peptide. The increased solubility and stability at low pH of the YSNSG cyclopeptide suggest that this peptide might be used as a potent antitumor therapeutic agent.

Experimental Procedures

Reagents

Culture reagents and molecular biology products were from Invitrogen (Cergy Pontoise, France). Bovine serum albumin, gelatin, and Matrigel (ECM gel) were purchased from Sigma (St-Quentin Fallavier, France). Human plasminogen was from Calbiochem (VWR International, Strasbourg, France). Anti-human MMP-14 and anti-human αVβ3 integrin antibodies (Chemicon, Euromedex, Souffelweyersheim, France) and anti-human PAI-1 antibody (American Diagnostica, Neuville sur Oise, France) were also used. The Biotrak ELISA evaluation kit of TIMP-2 and the enhanced chemiluminescence kit were from Amersham (Saclay, France).

Peptides

The native NC1[α3(IV)185–191] CNYYSNS peptide was obtained by solid-phase synthesis using an FMOC derivative procedure and was further purified by reverse phase HPLC with a C18 column by elution with a gradient of acetonitrile in trifluoroacetic acid, and

then lyophilized [12]. The synthesized YSNSG cyclopeptide was purchased from Ansynth Service B.V. (Roosendaal, The Netherlands). The native NC1[α3(IV)185–203] peptide was from Covalab (Oullins, France). For the determination of biological activities, the peptides were extemporaneously dissolved in dimethyl sulfoxide (DMSO); the final DMSO concentration was lower than 0.2% (v/v) in all experiments.

NMR

All NMR spectra were recorded on a Bruker DRX 500 spectrometer (Bruker, Wissembourg, France). The sample was dissolved in a 9:1 D_2O:H_2O mixture. TSP-d_4 was used as an internal chemical shift standard. Water proton signals were suppressed by the WATERGATE sequence. The chemical shift dependence of amide protons was studied at 294K, 300K, 305K, 310K, 315K, and 320K. The identification of the spin systems was achieved by analysis of the TOCSY spectrum (200 ms mixing time, mlevdpst19 pulse sequence). The classification of interproton distances was drawn from the NOESY spectrum (350 ms mixing time, noesygpst19 pulse sequence). The acquisition matrix of the latter contained 512 × 2048 data points, extended to 1024 × 4096 by zero filling. A cosine-squared apodization function was applied in both dimensions prior to 2D Fourier transformation.

Circular Dichroism

CD spectra of the YSNSG cyclopeptide were recorded on a JASCO J-810 CD spectropolarimeter (JASCO France, Bouguenais, France) equipped with a PTC-623S Peltier temperature control system by using a cell of 0.2 mm optical path length. The peptide was dissolved at a concentration of 400 μM either in water (pH 3) or in a 20 mM potassium phosphate buffer to bring the solution to pH 7. Three scans were accumulated in the spectral range of 190–250 nm at a temperature of 0°C, 20°C, 37°C, and 50°C by taking points every 0.1 nm.

Random Conformational Search of the YSNSG Cyclopeptide

We performed a random conformational search of the structure of the YSNSG cyclopeptide under NMR data constraints, in implicit water solvent, with a distance-dependent dielectric constant, by using the CHARMM program and force fields (PARAM set 22) [21, 22]. The geometrical distances corresponding to our experimentally observed nOes were constrained to be in the range of 2.0–4.0 Å. Additionally, distances between amide protons of the backbone that did not correlate were constrained to be in the range of 4.0–8.0 Å. Because we did not observe any Hα-Hα correlations in the NOESY spectrum (data not shown), all the peptide bonds were also constrained to be in *trans* conformation ($\omega \sim 180°$); finally, and in agreement with the Karplus relation modified by Pardi et al. [23], the φ angles of the two serine residues (S_2 and S_4) were also constrained around $-120° \pm 30°$ according to $^3J(N_H\text{-}H_\alpha)$ constant coupling values of 8.2 and 8.8 Hz, respectively (other residues shared values between 5.0 and 7.0 Hz).

At each step of our random conformational search protocol, we randomized all the backbone dihedral angles of the peptide and minimized the corresponding structure according to the NMR constraints described above. Each generated model was minimized using both Steepest Descent and Adopted Based Newton Raphson algorithms until an energy gradient of 10^{-5} kcal/mol was reached. Three fully independent runs of 1000 steps were performed by changing the initial seed of the random number generator. Finally, the 3000 generated minimized structures were grouped for analysis.

Molecular Dynamics Simulations

First, both the YSNSG linear and cyclopeptides were studied through MDS in water implicit solvent. The surface-accessible solvent area (SASA) model was used as a solvation model [24]. The solvent effect on the peptide included the EEF1 (energy effective function) model proposed by Lazaridis and Karplus [25]. Then, the peptides were studied in explicit solvent.

For the linear peptide, the starting point of the two MDSs was a fully extended conformation; for the cyclopeptide, the MDS started from the minimum energy conformations that were obtained either just after cyclization of the linear peptide or by the random conformational search described above. For MDS in explicit solvent, each peptide was first embedded in a water box ensuring 8 Å of water (TIP3P) on each of their sides. The systems were then energy minimized by 2000 steps of conjugate gradient and brought to room temperature (300K) by using the NAMD program [26, 27]. The two simulations were performed in the number of particles, pressure, and temperature (NPT) ensemble (1 atm; 300K) using the Verlet algorithm and an integration step of 10^{-15} s. Electrostatic interactions were treated by applying a switch function to the classical potential between 10 Å and 12 Å (cutoff value). A conformational analysis was performed on the full-length simulations that reached 20 ns, extracting the structures of the peptides each 10 ps of the trajectories. These models were grouped into a reduced number of clusters using NMRCLUST software [28] and a threshold of 2.5 Å for the clustering cutoff.

Animals

Female C57BL6 mice (average body weight, 18–20 g) were purchased from Harlan France (Gannat, France). Animals were individually caged and given food and water ad libitum. They were kept in a room with constant temperature and humidity. All mice were acclimatized to our laboratory conditions for 1 week before starting the experiments. The in vivo experiments were conducted according to the recommendations of the Centre National de la Recherche Scientifique.

Cell Cultures

B16F1 cells, a lung metastatic subline of murine B16 melanoma, were a generous gift from Dr. M. Grégoire (INSERM U419, Nantes, France). UACC-903 cells, a melanoma cell line, were from Dr. J. Trent (Georgetown University Medical Center, Washington, DC). B16F1 cells were cultured in RPMI 1640 and UACC-903 in Dulbecco's modified Eagle's medium (DMEM) containing glucose 4.5 g/l, both supplemented with 5% fetal bovine serum (FBS) in 25 cm^2 flasks (Nunclon, Dutscher, Brumath, France) under a humidified atmosphere of 5% CO_2 in air.

Cell Adhesion and Proliferation Measurements

Cell adhesion was measured on peptide-coated 96-well plates (Immunosorb, Nunclon, Dutscher, Brumath, France). Peptides were dissolved in DMSO and diluted in carbonate buffer (pH 10.0) and deposited onto 96-well plates at 4°C under sterile conditions. Cell adhesion was evaluated by absorbance at 560 nm after nuclei staining with crystal violet. For competition assays, cells were preincubated for 15 min with the competing peptides and then deposited onto peptide-coated 96-well plates as described above.

Cell proliferation was determined using WST-1 reagent according to the manufacturer's instructions (Roche Diagnostics, Meylan, France). In all experiments, cell viability was greater than 98%, as assessed by trypan blue exclusion.

In Vitro Invasion Assays

Invasion was assayed in modified Boyden chambers (ThinCert, tissue culture insert for 24-well plates, 8.36 mm inner diameter, 8 μm pore, Greiner Bio-one, Courtaboeuf, France) as previously described [11].

Zymography Analyses

Cell Incubation with the Peptides

At subconfluence, cells were washed twice with phosphate-buffered saline to remove residual FBS and incubated for 48 hr in DMEM, with or without the peptides, at concentrations ranging from 0 to 20 μM. Conditioned media were harvested and centrifuged at 500 × g for 10 min at 4°C to remove cellular debris. Protein contents of the media were determined by the Bradford method, using bovine serum albumin as a standard [29].

Gelatin Zymography

The expression and activation of pro-MMP-2 and pro-MMP-9 in conditioned media or in cell membrane extracts of UACC-903 cells, treated or not with the peptides, were analyzed by gelatin zymography as previously described [11].

The secretion of TIMP-2 was analyzed on UACC-903-conditioned media by reverse gelatin zymography as previously described [11]. TIMP-2 secretion was also measured using a Biotrak ELISA kit, according to the manufacturer's instructions.

Gelatin-Plasminogen Zymography

For the determination of plasminogen activators, UACC-903-conditioned media were analyzed on SDS-polyacrylamide gels containing 1 mg/ml gelatin and 10 μg/ml plasminogen as previously described [30].

Western Blot Analysis

Samples were electrophoresed in a 0.1% SDS, 10% polyacrylamide gel. They were then transferred onto Immobilon-P membranes (Millipore, St Quentin en Yvelines, France). The membranes were blocked with 5% nonfat dry milk, 0.1% Tween 20 in a 50 mM Tris-HCl buffer, 150 mM NaCl (pH 7.5) (TBS) for 2 hr at room temperature and incubated overnight at 4°C with anti-MMP-14 or anti-PAI-1 antibody and then for 1 hr at room temperature with a second peroxidase-conjugated anti-IgG antibody. Immune complexes were visualized with the enhanced chemiluminescence detection kit.

In Vivo Tumor Growth Measurement

Suspensions of B16F1 cells (2.5×10^5 cells in 0.1 ml RPMI 1640 medium) were subcutaneously injected into the left side of different series of syngenic C57BL6 mice. Tumors appeared at day 6 and intraperitoneal administrations of peptides were performed at day 6, 8, and 11. Tumor sizes were measured every 2 days. Tumor volume was determined according to $v = 0.5\ A \times B^2$, where A denotes the largest dimension of the tumor and B represents the smallest dimension [31].

Statistical Analyses

All in vitro experiments were done in quadruplicate. Statistical analyses were performed by Student's t test. Results were expressed as mean ± 1 standard deviation. For in vivo experiments, volumes of primary tumors were statistically analyzed using the nonparametric *u*-test of Mann and Whitney and the parametric Student's t test paired with weight-matched mice.

Supplemental Data

Supplemental Data include one figure and can be found with this article online at http://www.chembiol.com/cgi/content/full/13/12/1307/DC1/.

Acknowledgments

The authors thank D. Patigny and J.Y. Laronze (CNRS FRE 2715, UFR Pharmacie, Reims) for their expertise in synthesis of the native CNYYSNS peptide. They also thank S. Gobert (University of Reims Champagne-Ardenne) for improving the English language of the manuscript. This work was supported by grants from the Centre National de la Recherche Scientifique (UMR 6198), the University of Reims Champagne-Ardenne, the Association pour la Recherche sur le Cancer, the Association Régionale pour l'Enseignement Supérieur et la Recherche Scientifique et Technologique en Champagne-Ardenne (ARERS-Verre Espoir), the Ligue Nationale Contre le Cancer (Comités de l'Aisne et de la Haute-Marne), and the Canceropole Grand Est.

Received: July 25, 2006
Revised: October 12, 2006
Accepted: October 13, 2006
Published: December 22, 2006

References

1. Egeblad, M., and Werb, Z. (2002). New functions for the matrix metalloproteinases in cancer progression. Nat. Rev. Cancer *2*, 161–174.
2. Hofmann, U.B., Houben, R., Bröcker, E.B., and Becker, J.C. (2005). Role of matrix metalloproteinases in melanoma cell invasion. Biochimie *87*, 307–314.
3. Itoh, Y., and Seiki, M. (2006). MT1-MMP: a potent modifier of pericellular microenvironment. J. Cell. Physiol. *206*, 1–8.
4. Seiki, M. (2003). Membrane-type 1 matrix metalloproteinase: a key enzyme for tumor invasion. Cancer Lett. *194*, 1–11.
5. Brooks, P.C., Stromblad, S., Sanders, L.C., von Schalscha, T.L., Aimes, R.T., Stetler-Stevenson, W.G., Quigley, J.P., and Cheresh, D.A. (1996). Localization of matrix metalloproteinase MMP-2 to the surface of invasive cells by interaction with integrin α v β 3. Cell *85*, 683–693.
6. Andreasen, P.A., Egelund, R., and Petersen, H.H. (2000). The plasminogen activation system in tumor growth, invasion, and metastasis. Cell. Mol. Life Sci. *57*, 25–40.
7. Monea, S., Lehti, K., Keski-Oja, J., and Mignatti, P. (2002). Plasmin activates pro-matrix metalloproteinase-2 with a membrane-type 1 matrix metalloproteinase-dependent mechanism. J. Cell. Physiol. *192*, 160–170.
8. Sado, Y., Kagawa, M., Naito, I., Ueki, Y., Seki, T., Momota, R., Oohashi, T., and Ninomiya, Y. (1998). Organization and expression of basement membrane collagen IV genes and their roles in human disorders. J. Biochem. (Tokyo) *123*, 767–776.
9. Ortega, N., and Werb, Z. (2002). New functional roles for non-collagenous domains of basement membrane collagens. J. Cell Sci. *115*, 4201–4214.
10. Maeshima, Y., Colorado, P.C., Torre, A., Holthaus, K.A., Grunkemeyer, J.A., Ericksen, M.B., Hopfer, H., Xiao, Y., Stillman, I.E., and Kalluri, R. (2000). Distinct antitumor properties of a type IV collagen domain derived from basement membrane. J. Biol. Chem. *275*, 21340–21348.
11. Pasco, S., Han, J., Gillery, P., Bellon, G., Maquart, F.X., Borel, J.P., Kefalides, N.A., and Monboisse, J.C. (2000). A specific sequence of the noncollagenous domain of the α3(IV) chain of type IV collagen inhibits expression and activation of matrix metalloproteinases by tumor cells. Cancer Res. *60*, 467–473.
12. Floquet, N., Pasco, S., Ramont, L., Derreumaux, P., Laronze, J.Y., Nuzillard, J.M., Maquart, F.X., Alix, A.J.P., and Monboisse, J.C. (2004). The antitumor properties of the α3(IV)-(185–203) peptide from the NC1 domain of type IV collagen (tumstatin) are conformation-dependent. J. Biol. Chem. *279*, 2091–2100.
13. Fuchs, P.F.J., and Alix, A.J.P. (2005). High accuracy prediction of β-turns and their types using propensities and multiple alignments. Proteins *59*, 828–839.
14. Essmann, U., Perera, L., Berkowitz, M.L., Darden, T., Lee, H., and Pedersen, L.G. (1995). A smooth particle mesh Ewald method. J. Chem. Phys. *103*, 8577–8593.
15. Humphrey, W., Dalke, A., and Schulten, K. (1996). VMD: visual molecular dynamics. J. Mol. Graph. *14*, 33–38, 27–28.
16. Pasco, S., Monboisse, J.C., and Kieffer, N. (2000). The α3(IV)185–206 peptide from noncollagenous domain 1 of type IV collagen interacts with a novel binding site on the β3 subunit of integrin αVβ3 and stimulates focal adhesion kinase and phosphatidylinositol 3-kinase phosphorylation. J. Biol. Chem. *275*, 32999–33007.
17. Sato, H., Takino, T., and Miyamori, H. (2005). Roles of membrane-type matrix metalloproteinase-1 in tumor invasion and metastasis. Cancer Sci. *96*, 212–217.
18. Kim, J., Hong, S.Y., Park, H.S., Kim, D.S., and Lee, W. (2005). Structure and function of RGD peptides derived from disintegrin proteins. Mol. Cells *19*, 205–211.
19. Buerkle, M.A., Pahernik, S.A., Sutter, A., Jonczyk, A., Messmer, K., and Dellian, M. (2002). Inhibition of the α-V integrins with a cyclic RGD peptide impairs angiogenesis, growth and metastasis of solid tumours in vivo. Br. J. Cancer *86*, 788–795.
20. Haier, J., Goldmann, U., Hotz, B., Runkel, N., and Keilholz, U. (2002). Inhibition of tumor progression and neoangiogenesis using cyclic RGD-peptides in a chemically induced colon carcinoma in rats. Clin. Exp. Metastasis *19*, 665–672.
21. Brooks, B.R., Bruccoleri, R.E., Olafson, B.D., States, D.J., Swaminathan, S., and Karplus, M. (1983). CHARMM: a program for macromolecular energy, minimization, and dynamics calculations. J. Comput. Chem. *4*, 187–217.
22. MacKerell, A.D., Jr., Bashford, D., Bellott, M., Dunbrack, R.L., Jr., Evanseck, J.D., Field, M.J., Fischer, S., Gao, J., Guo, H., Ha, S., et al. (1998). All-atom empirical potential for molecular modeling and dynamics studies of proteins. J. Phys. Chem. B *102*, 3586–3616.
23. Pardi, A., Billeter, M., Jr., and Wuthrich, K. (1984). Calibration of the angular dependence of the amide proton-C α proton coupling constants, ^{3}JHN α, in a globular protein. Use of ^{3}JHN α for identification of helical secondary structure. J. Mol. Biol. *180*, 741–751.

24. Ferrara, P., Apostolakis, J., and Caflisch, A. (2002). Evaluation of a fast implicit solvent model for molecular dynamics simulations. Proteins *46*, 24–33.
25. Lazaridis, T., and Karplus, M. (1999). Effective energy function for proteins in solution. Proteins *35*, 133–152.
26. Phillips, J.C., Braun, R., Wang, W., Gumbart, J., Tajkhorshid, E., Villa, E., Chipot, C., Skeel, R.D., Kale, L., and Schulten, K. (2005). Scalable molecular dynamics with NAMD. J. Comput. Chem. *26*, 1781–1802.
27. Kalé, L., Skeel, R., Bhandarkar, M., Brunner, R., Gursoy, A., Krawetz, N., Phillips, J., Shinozaki, A., Varadarajan, K., and Schulten, K. (1999). NAMD2: greater scalability for parallel molecular dynamics. J. Comput. Phys. *151*, 283–312.
28. Kelley, L.A., Gardner, S.P., and Sutcliffe, M.J. (1996). An automated approach for clustering an ensemble of NMR-derived protein structures into conformationally related subfamilies. Protein Eng. *9*, 1063–1065.
29. Bradford, M.M. (1976). A rapid and sensitive method for the quantitation of microgram quantities of protein utilizing the principle of protein-dye binding. Anal. Biochem. *72*, 248–254.
30. Pasco, S., Ramont, L., Venteo, L., Pluot, M., Maquart, F.X., and Monboisse, J.C. (2004). In vivo overexpression of tumstatin domains by tumor cells inhibits their invasive properties in a mouse melanoma model. Exp. Cell Res. *301*, 251–265.
31. Wald, M., Olejar, T., Sebkova, V., Zadinova, M., Boubelik, M., and Pouckova, P. (2001). Mixture of trypsin, chymotrypsin and papain reduces formation of metastases and extends survival time of C57Bl6 mice with syngeneic melanoma B16. Cancer Chemother. Pharmacol. Suppl. *47*, S16–S22.